Applied Nanoscience (2022) 12:3197–3206
https://doi.org/10.1007/s13204-021-02328-y

ORIGINAL ARTICLE

g-C_3N_4/TiO_2 nanocomposite photocatalyst for methylene blue photodegradation under visible light

Mohd Hasmizam Razali[1,2] · Muhammad Amir Fikri Md Fauzi[2] · Basirah Mohd Azam[2] · Mahani Yusoff[3]

Received: 6 January 2021 / Accepted: 19 December 2021 / Published online: 3 February 2022

Abstract

In this research, the g-C_3N_4/TiO_2 nanocomposite was prepared by a simple hydrothermal method and was used as photocatalyst for dye degradation. Prior to that, the g-C_3N_4/TiO_2 was characterized by different analytical techniques such as FTIR, XRD, SEM, and nitrogen gas adsorption. Main functional groups of g-C_3N_4/TiO_2 composite are shown in the FTIR spectrum. The XRD pattern reveals that the presence of anatase and rutile phases of TiO_2 as well as layer stacking of conjugated aromatic and in-planar repeating triazine unit of g-C_3N_4. The SEM analysis shows the presence of 2D-layered structured of g-C_3N_4 and agglomerated spherical TiO_2 particles (0D). The 2D/0D g-C_3N_4/TiO_2 nanocomposite shows higher photocatalytic activity than pure g-C_3N_4 and TiO_2, whereby 100% of MB was degraded under visible light after 2 h. This is attributed to their high surface area which is 273.32 mg^{-1} and generation of more effective reactive oxygen species of •OH and •O_2 to degrade MB.

Keywords Nanocomposite · Photocatalyst · Degradation · Dye · Visible light

Introduction

Photocatalytic degradation of organic pollutant using nanostructured materials had become an interesting research area by researchers worldwide. This is because of their explicit advantages, including high surface areas, effective charge separation, directional charge transport, and light trapping/scattering effects (Sun et al. 2020). In particular, nanostructured titanium dioxide (TiO_2) such as zero-dimensional (0D), one-dimensional (1D), two-dimensional (2D) and three-dimensional (3D)/hierarchical have been explored and tested as photocatalyst for degradation of various dyes. It is well published that 0D materials like TiO_2 nanoparticle managed to degrade Congo red (CR) dye completely after 80 min of continuous illumination (Sathiyan et al. 2020; Li et al. 2019a; Goutam et al. 2018). Recently, researcher reported that 1D TiO_2 nanotubes doped with copper shows high photocatalytic activity with 90% degradation of methyl orange after 180 min (Razali et al. 2020a). On top of that, it was also found that 3D TiO_2 nanocomposite is not only capable to degrade methyl orange dye but also could be used in biomedical application for cell growth and as an antibacterial material (Razali et al. 2018). Even though the performance of nanostructured TiO_2 materials is good somehow, they are not efficient enough since pure nanostructured TiO_2 materials work only under UV light due to their large bandgap energy and fast-recombination thus slowing their photocatalytic activity rate. Thus, combination with low bandgap energy of organic semiconductor was proposed to enhance their photocatalytic activity under visible light. Recently, graphitic carbon nitride (g-C_3N_4) has been reported to be a promising candidate for photocatalysis due to their low bandgap energy and easily prepared at low cost (Gahlot et al. 2021; Kang et al. 2018; Zhang et al. 2017). The 2D-layered structure of g-C_3N_4 similar to graphene with conjugated system benefits the transport of charge carriers and their low bandgap energy of ~ 2.7 eV endows the polymeric semiconductor with visible light-absorbing ability up to 460 nm (Chen et al. 2020; Hong et al. 2020). Strong

✉ Mohd Hasmizam Razali
mdhasmizam@umt.edu.my

1 Advanced Nanomaterials Research Group, Faculty of Science and Marine Environment, Universiti Malaysia Terengganu, 21030 Kuala Nerus, Terengganu, Malaysia

2 Faculty of Science and Marine Environment, Universiti Malaysia Terengganu, 21030 Kuala Nerus, Terengganu, Malaysia

3 Faculty of Bioengineering and Technology, Universiti Malaysia Kelantan, 17600 Jeli, Kelantan, Malaysia

covalent bonds between carbon with nitride atoms and tris-trizaine (C_6N_7)-based building blocks in the molecular structure of g-C_3N_4, made them thermally and photochemically stable semiconductor (Chegeni et al. 2020; Muhmood and Uddin 2020; Li et al. 2019b). Therefore, due to their unique properties, 2D-layered g-C_3N_4 was combined with 0D TiO_2 nanoparticles to produce 2D/0D heterostructures g-C_3N_4/TiO_2 nanocomposite photocatalyst. The synthesized 2D/0D nanocomposite photocatalyst was characterized using various instruments to study their physical and chemical properties. Then, the performance of the photocatalyst was tested for methylene blue (MB) degradation.

Experimental

Materials and reagents

All chemicals are the analytical grade (AR) and used without any further purification. Urea powder (NH_2CONH_2; AR, ≥ 99.0%), titanium tetrachloride ($TiCl_4$, AR, ≥ 99.0%) and sulphuric acid (H_2SO_4, AR, ≥ 99.0%), benzoquinone ($C_6H_4(=O)_2$: AR, ≥ 98.0%) and isopropyl alcohol ($(CH_3)_2CHOH$; AR, ≥ 99.7%) were purchased from Sigma-Aldrich.

Preparation of layered g-C_3N_4

Bulk g-C_3N_4 was produced via a thermal poly-condensation method. Typically, 20 g of urea was placed into a ceramic crucible with a cover and heated in a furnace at 550 °C for 4 h with heating rate 5 °C per min. After cooling down naturally, the coarse solid products were collected and well ground into powder with the size around 180 µm in a mortar. To prepare layered g-C_3N_4, 1 g of bulk g-C_3N_4 was put into a beaker with 20 mL of concentrated sulphuric acid and magnetically stirred for 8 h at room temperature to ensure that the bulk g-C_3N_4 was exfoliated into layered g-C_3N_4 completely. Subsequently, the sticky mixture of g-C_3N_4 and sulphuric acid was poured into 100 mL of distilled water and then transferred to a water bath for another 8 h of magnetic stirring at a specific temperature of 80 °C to remove the excess sulphuric acid. The resulting suspension was centrifuged to separate the solid particulates from liquid. The solid was washed by replacing the liquid after centrifuging with distilled water and was centrifuged again for 2 times. Finally, the collected solid sample was dried to obtain layered g-C_3N_4.

Preparation of g-C_3N_4/TiO_2 photocatalyst

The obtained layered g-C_3N_4 was weighted for 1.0 g and poured into a beaker with 100 mL of distilled water. The mixture was stirred to be homogeneous for 10 min. 20 mL of titanium tetrachloride ($TiCl_4$) was poured into the solution mixture immediately in fume hood, because it is a volatile liquid and easily vaporized. The solution was stirred further for 20 min and dried in oven for 24 h at 70 °C. After drying, the powder sample was annealed at 400 °C for 1 h with rate of 20 °C/min. The yellowish white powder obtained was labeled as g-C_3N_4/TiO_2. TiO_2 nanoparticle was prepared using similar procedure without the addition of g-C_3N_4 solution.

Characterization of sample

Fourier transform infrared (FTIR) spectroscopy was used to study the functional group of sample. FTIR spectra were conducted on Niconet 5700 FTIR spectrometer with the sample was dispersed in potassium bromide (KBr). The analysis was done from 400 to 4000 cm^{-1} wavenumber. X-ray diffraction (XRD) was utilized to study the crystal structure and the XRD patterns were acquired on Bruker D8 Advance X-ray diffractometer (Bruker AXS, German) at a scanning speed of 0.2 s^{-1} from 10 to 90° of 2θ. The morphology of the sample was captured by ZEISS SUPRA™ 35VP scanning electron microscope (SEM). Micromeritics ASAP 2000 instrument was used for the nitrogen gas adsorption analysis at the temperature of − 196 °C (boiling temperature of liquid nitrogen) to determine the Brunauer, Emmett and Teller (BET) surface area and porosity. For sample preparation, the powder sample of about 1.5 mg was poured into glass tube. The prepared sample in glass tube was degassed at 300 °C for 5 h under vacuum to remove the previously absorbed contaminant on the surface and pores of the samples before measurement.

Photocatalytic activity study

First, 10 mg powder of each photocatalyst was separately dispersed in 60 mL dye aqueous solution at a specific concentration (5 ppm). Preceding to the photocatalytic test, the mixture solution was stirred magnetically in dark for 1 h to attain adsorption/desorption equilibrium between dye and photocatalyst. A specific solution (5 mL) of initial concentration (C_o) was taken out, and then, the solution was exposed to visible light with a 300 W halogen lamp with a UV cutoff filter. The distance between solution and lamp was 5 cm. During the reaction process, reactant mixtures were continuously stirred and samples were extracted after regular intervals (30 min) to define the degradation of dye. The extracted samples were centrifuged at 6000 rpm for 10 min for solid–liquid separation and to remove suspensions. Temporal concentrations variation of MB dye was monitored by investigating the change in absorption peaks at 665 nm using the UV–Vis spectrometer (Perkin Elmer

Lambda 35 UV–Vis). The photodegradation efficiency (η) was calculated using the following equation:

$$\text{Degradation}(\eta) = \frac{C_0 - C_t}{C_0} \times 100, \quad (1)$$

where C_0 is the initial absorption of MO and C_t is the absorption of MO after the reaction at t time. The photocatalytic testing was replicated for 3 times.

Photocatalytic mechanistic investigation

To explore the exact mechanistic pathway of MB photocatalytic degradation using the g-C_3N_4/TiO_2 nanocomposite under visible-light irradiation, 0.1 mmol of quenchers such as benzoquinone (BQ) and isopropyl alcohol (IPA) were added in the reaction system for superoxide radicals ($O_{2\bullet}^-$) and hydroxyl radical (OH•) trapping, respectively.

Results and discussion

Figure 1 shows the FTIR spectra of prepared photocatalyst samples. For TiO_2 sample, a broad peak observed within 1500–500 cm^{-1} is due to the metal and oxygen bond corresponding to Ti–O stretching vibration (Razali et al. 2020b). The peaks at 1641.42 cm^{-1} and 3400–3500 cm^{-1} were corresponding to hydroxyl group of physically adsorbed water (Razali and Yusof 2018). For g-C_3N_4, it has a strong characteristic peak at 813 cm^{-1}, which is part of the bending vibration of the triazine rings (Zheng et al. 2020). In addition, several absorption bands ascribing to the representative stretching mode of the carbon nitride aromatic ring were also detected in the range of 1000 to 2000 cm^{-1}. Among them, 1240 and 1317 cm^{-1} are pertained to the stretching vibration of the C–N, H–C and C–N (–C)–C connecting unit (Tian et al. 2013). The peaks at 1408 cm^{-1}, 1461 cm^{-1} and 1641 cm^{-1} are due to the stretching vibration of CN in the g-C_3N_4 structure (Dong et al. 2013). Lastly, a broad peak at region of 2500–3600 cm^{-1} indicates the stretching vibration modes of the terminal NH groups, as reported by other researchers (Li et al. 2020; Wang et al. 2019). While, within 1240–1570 cm^{-1} region is an aromatic C–N bonds (Tan et al. 2019). For the g-C_3N_4/TiO_2 hybrid sample, their spectra clearly show the main characteristic of both g-C_3N_4 and TiO_2. For instance, broad peak at 2500–3700 cm^{-1} is assigned to N–H stretching and the peaks of Ti–O–Ti and Ti–O stretching within 1100–500 cm^{-1} (Hao et al. 2020). However, these peaks shifted to red shift as compared to pure TiO_2 sample. This phenomenon is attributed to a decrease in the vibrational energy of the Ti–O–Ti and Ti–O bonds. It means that the bond strength is weakened, suggesting that a strong interaction at the interfacial contact between these two compounds, which further confirms the successful preparation of the g-C_3N_4/TiO_2 nanocomposites. Furthermore, the appearance of sharp peak at 1631.78 cm^{-1} which is attributed to the stretching vibrations of C–N and C=N heterocyclic unit confirm the presence of g-C_3N_4 in the g-C_3N_4/TiO_2 nanocomposite sample (Hao et al. 2020).

The XRD pattern of pure g-C_3N_4, TiO_2 and g-C_3N_4/TiO_2 nanocomposite are shown in Fig. 2. Two broad peaks were observed at 13.48° and 27.55° for pure g-C_3N_4 sample (Fig. 2a). First peak is corresponding to the (1 0 0) crystal plane of the in-planar repeating triazine unit. Meanwhile second peak was indexed as (0 0 2) crystal plane of layer stacking of conjugated aromatic system (JCPDS: 87–1526), as reported previously by other researchers (Tan et al. 2019; Dong et al. 2014). While in Fig. 2b, pure TiO_2 sample displays sharp and narrow peaks at 27.52°, 36.2°, 39.26°,

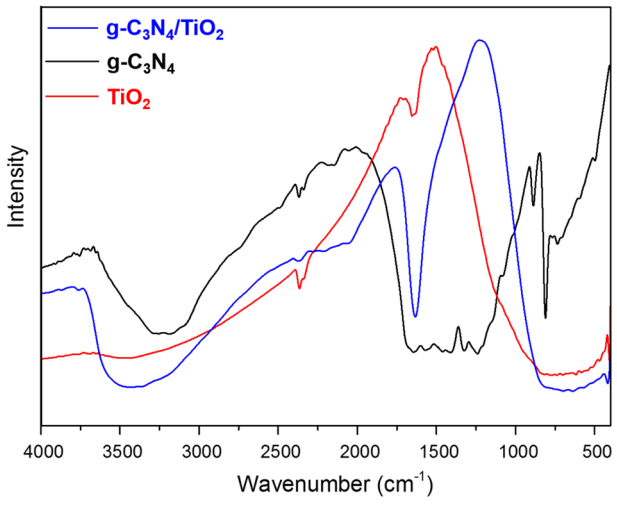

Fig. 1 FTIR spectra of pure g-C_3N_4, TiO_2 and g-C_3N_4/TiO_2 nanocomposite photocatalyst

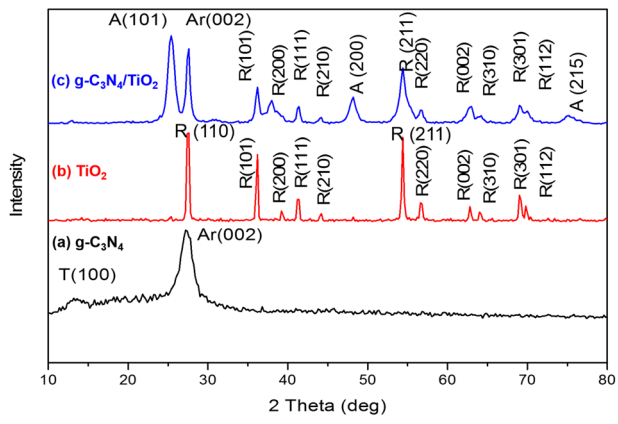

Fig. 2 XRD patterns of **a** pure g-C_3N_4 **b** TiO_2 and **c** g-C_3N_4/TiO_2 nanocomposite photocatalyst

41.3°, 44.08°, 54.36°, 56.72°, 62.78°, 64.1°, 69.02° and 69.78° which are assigned to the (110), (101), (200), (111), (210), (211), (220), (002), (310), (301) and (112) rutile TiO_2 (JCPDS: 21–1276) (Warkhade et al. 2019; Fang et al. 2020). For g-C_3N_4/TiO_2 nanocomposite sample (Fig. 3c), similar XRD pattern was observed as pure g-C_3N_4 and TiO_2 except the addition of new peaks at 25.4°, 48.6° and 75.4° which are assigned to (101), (200), (215) anatase TiO_2, respectively (JCPDS: 21-1272). The appearance of the anatase TiO_2 peaks was due to the chemical interaction between g-C_3N_4 and TiO_2, which confirms the g-C_3N_4/TiO_2 heterojunction formation. On top of that, as can be seen in XRD pattern the peak of the interlayer stacking of g-C_3N_4 aromatic segments and rutile TiO_2 is overlapped thus resulted in formation of broader peak in g-C_3N_4/TiO_2 nanocomposite sample at ~ 27°, as compared to pure g-C_3N_4 sample. This phenomena suggested the produced sample is composed of both g-C_3N_4 and TiO_2. The appearance of new peak of anatase TiO_2 for nanocomposite sample is interesting since the existence of both phase of TiO_2 which are anatase and rutile can enhance the photocatalytic activity (Antunes et al. 2020).

The SEM images of studied samples are shown in Fig. 3. Layered structures are observed in Fig. 3a, suggesting that sheet-like g-C_3N_4 (2D) was successfully synthesized using hydrothermal method. The thickness of sheet-like structure was found to be ≤ 100 nm. Meanwhile, the TiO_2 shows the

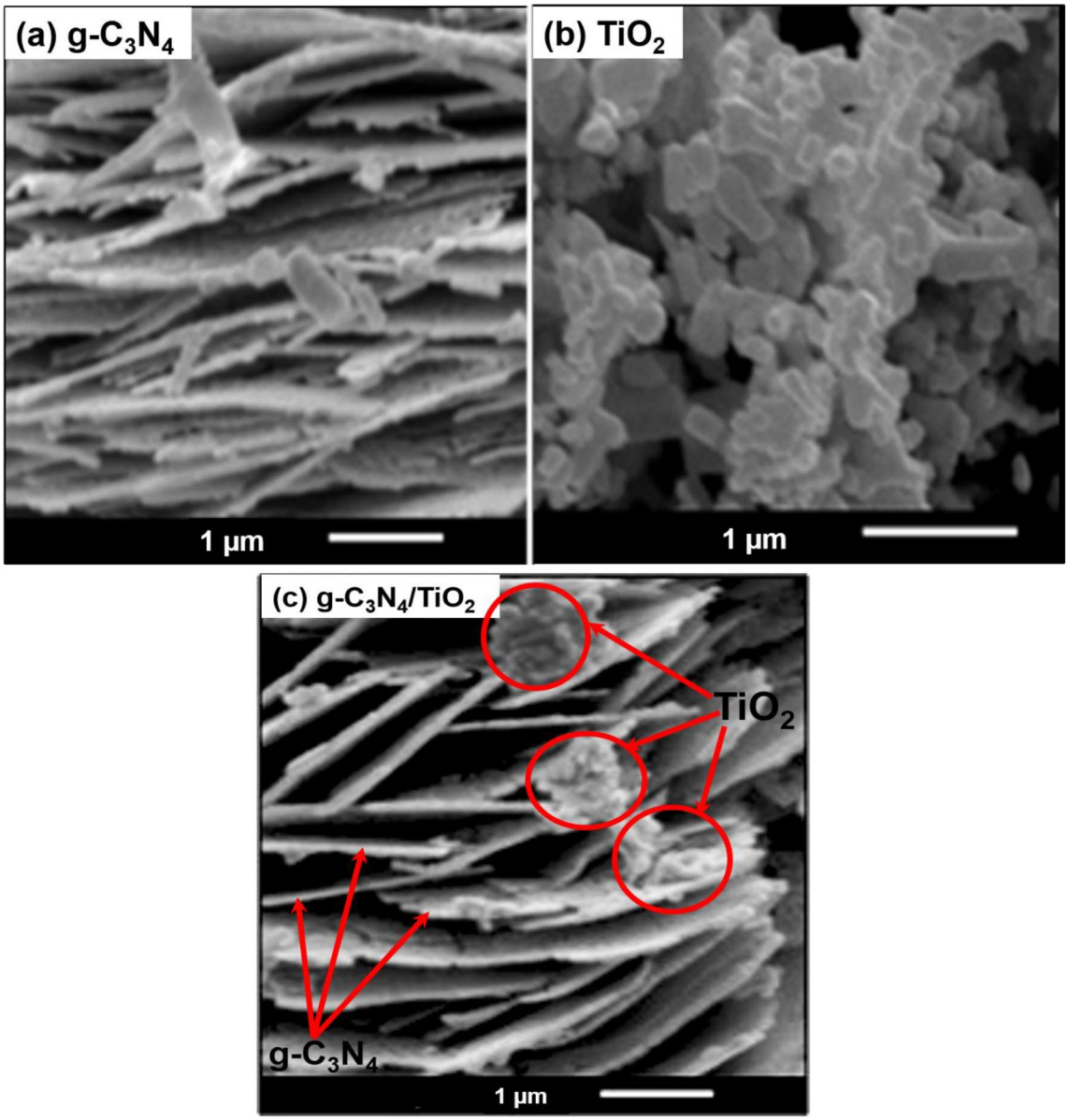

Fig. 3 SEM micrographs of **a** pure g-C_3N_4 **b** TiO_2 and **c** g-C_3N_4/TiO_2 nanocomposite photocatalyst

irregular shape particles with the size within 60–80 nm as observed in Fig. 3b. The nanoparticles were found to be agglomerated to form bulk particles due to the heating process during the preparation step. The nanoparticles are uniformly wrapped on the surface of the layered g-C_3N_4 in the g-C_3N_4/TiO_2 composite (Fig. 3c).

Figure 4 shows the nitrogen adsorption–desorption isotherm plot of pure g-C_3N_4, TiO_2 and g-C_3N_4/TiO_2 nanocomposite. The isotherm for all studied samples exhibit a typical IV-like isotherm with H3 hysteresis according to IUPAC classification (Abdelraheem et al. 2019; Ahmed et al. 2017). Type IV isotherms are usually associated with capillary condensation in mesopore structures. Mesoporous structures are encountered with materials having pores in the general range of 2–50 nm. As shown in Table 1, the pore sizes of the samples are between 8.88 and 32.92 nm, which is in the mesopore range suggesting very narrow distributions of the mesopore dimensions. The surface area of pure g-C_3N_4, TiO_2 and g-C_3N_4/TiO_2 nanocomposite was found to be 73.42, 186.48, and 273.32 m^2/g, respectively, suggesting that more pores were produced in TiO_2 and g-C_3N_4/TiO_2 nanocomposite sample (Table 1). This is due to the small size particle of near-spherical TiO_2 nanomaterials used in this research. Smaller spherical TiO_2 nanoparticles will produce high numbers of particles and pores. The pore volume and pore size of the g-C_3N_4, TiO_2 and g-C_3N_4/TiO_2 nanocomposite is tabulated in Table 1. BJH pore-size distribution of the studied samples can be observed in Fig. 4 (insert). A broad BJH pore-size distribution curve of pure g-C_3N_4 within 20–80 nm is a wide pore-size distribution proposing that g-C_3N_4 composed of both macropore and mesopore

Table 1 BET surface area, pore volume and pore size of pure g-C_3N_4, TiO_2 and g-C_3N_4/TiO_2 nanocomposite

Sample	Surface area (m^2/g)	Pore volume (cm^3/g)	Pore size (nm)
g-C_3N_4	73.42	0.167	32.92
TiO_2	186.48	1.240	8.88
g-C_3N_4/TiO_2	273.32	1.720	21.99

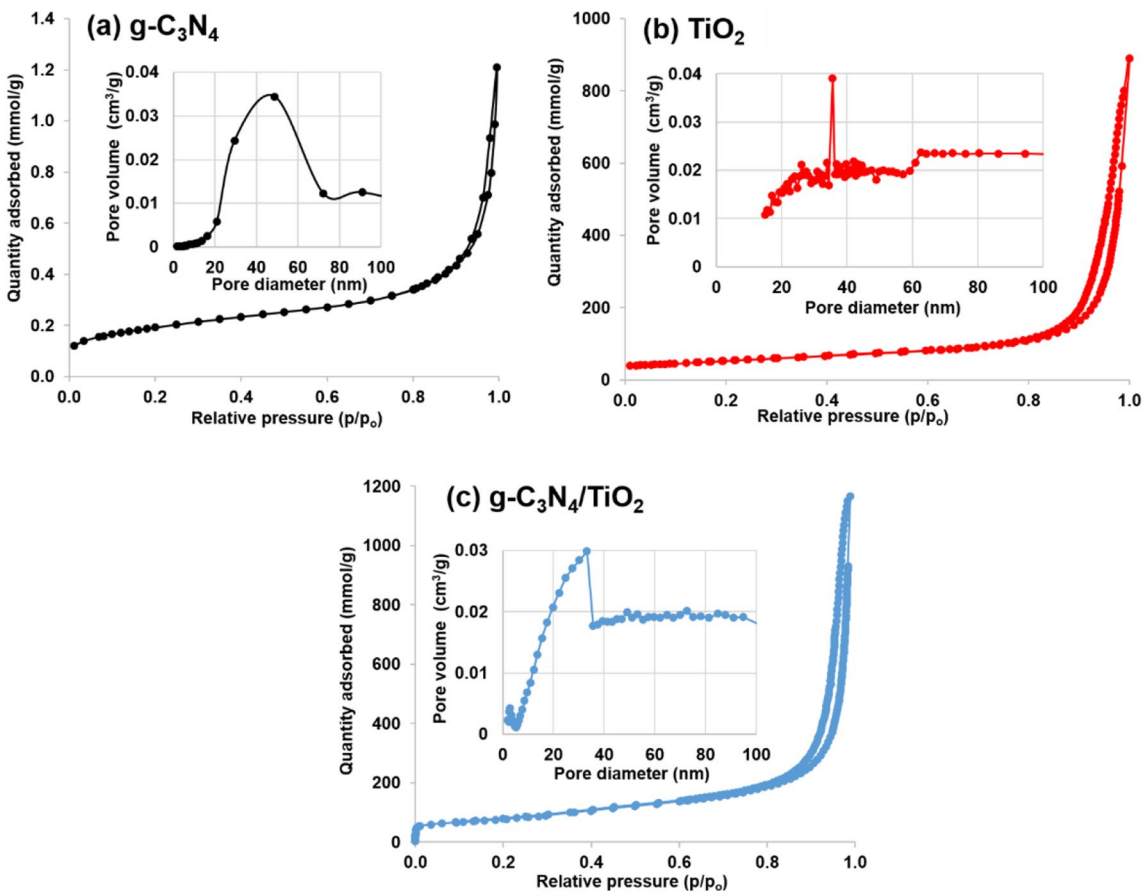

Fig. 4 Nitrogen adsorption/desorption isotherms and BJH pore-size distribution profiles (inset) of **a** pure g-C_3N_4, **b** TiO_2 and **c** g-C_3N_4/TiO_2 nanocomposite photocatalyst

structures. This is attributed to their layered structures. On the other hand, narrow pore-size distribution was observed for spherical TiO_2 nanoparticles sample. The average of pore diameter is about 33–37 nm. Interestingly, both pattern which are wide (5–33) nm and narrow (34–35) nm pore-size distribution was obtained for g-C_3N_4/TiO_2 nanocomposite sample proved the existence of layered and nanoparticle pores. Moreover, the pore-size distribution of nanocomposite sample is only in mesopore range proposing that TiO_2 nanoparticle was loaded onto layered g-C_3N_4 to create only mesopores. These type of pores were expected to provide a good adsorption and active site for degradation of MB.

The degradation was carried out under visible light using synthesized g-C_3N_4/TiO_2 nanocomposite, pure g-C_3N_4 and TiO_2. After 120 min, complete degradation (100%) of MB was achieved for g-C_3N_4/TiO_2 nanocomposite. While, 49.06% of MB was degraded using pure g-C_3N_4 and single TiO_2 was managed to degrade only 10.20% (Fig. 5a). As well known, TiO_2 is not active under visible light, thus low degradation was obtained due to the adsorption of MB into the TiO_2 surface and photolysis of MB (3.80%). High photocatalytic capability of g-C_3N_4/TiO_2 nanocomposite was due

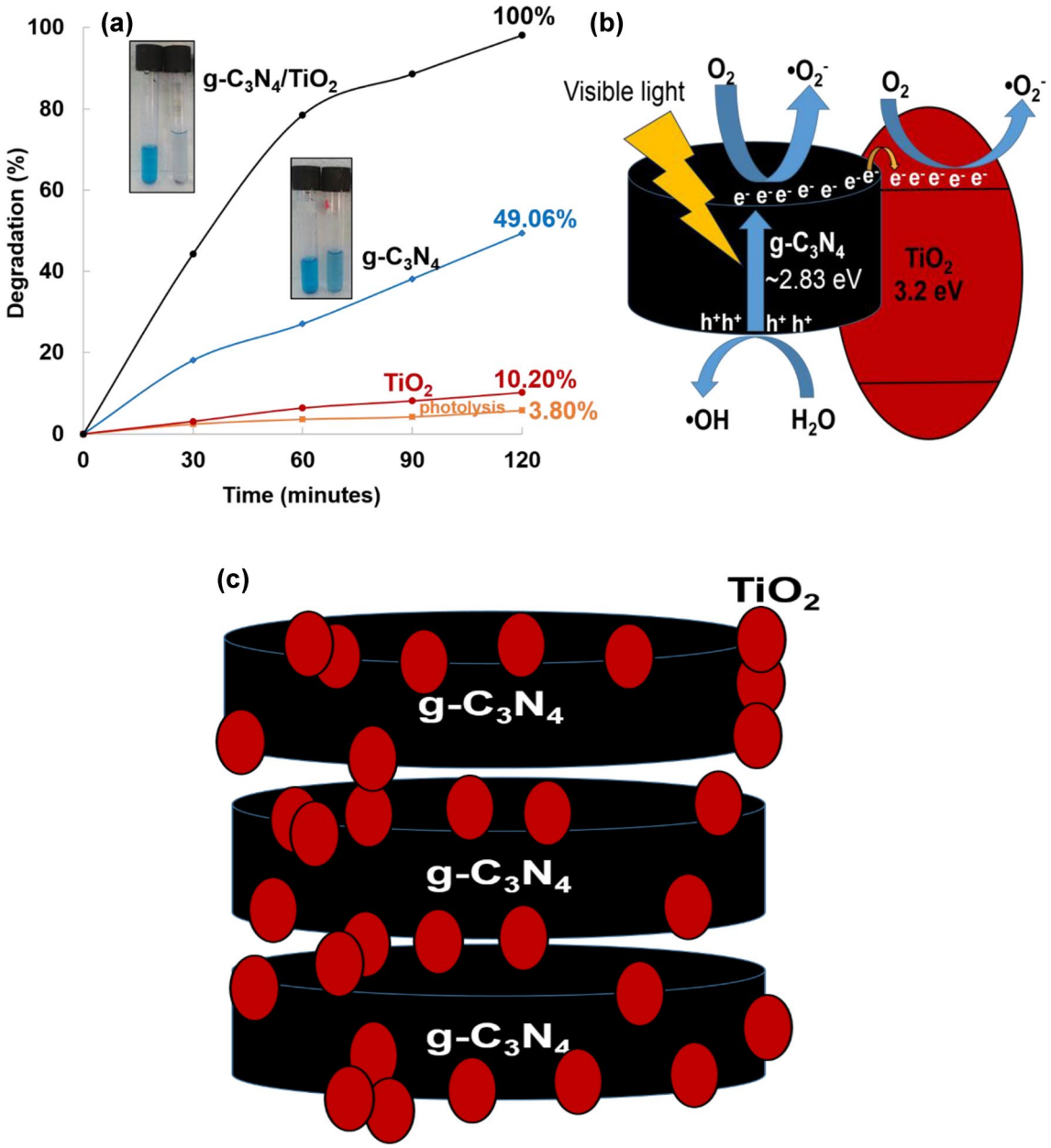

Fig. 5 **a** Degradation rate, **b** mechanism of interphase charge transfer, and (**c**) nano-spherical inter-layered of g-C_3N_4/TiO_2 photocatalyst

to the interface charge transfer between g-C_3N_4 and TiO_2, which can prevent the recombination of electron and positive hole charges (Fig. 5b). On top of that, large BET surface of g-C_3N_4/TiO_2 nanocomposite which is attributed to their layered and nano-spherical structures (Fig. 5c), thus could produce more reactive oxygen species (ROS) such as hydroxyl radical (•OH) and superoxide radicals (•O_2) to degrade the MB compound. For comparison, the photocatalytic activity of synthesized g-C_3N_4/TiO_2 nanocomposite and other photocatalyst for degradation of MB under visible-light irradiation is listed in Table 2. The TiO_2/g-C_3N_4 nanocomposite exhibits better or comparable photocatalytic activity in MB degradation.

The bandgap energy of g-C_3N_4/TiO_2 nanocomposite was determined using UV–Vis. A graph of $[\ln (R_{max} - R_{min}/R - R_{min})]^2$ versus photon energy (bandgap energy, Eg) was plotted, where R_{max} represents the maximum reflectance value in the desired wavelength and R_{min} represents the minimum reflectance value in desired wavelength. The energy bandgap was determined based on the intersection from the extrapolation of the straight line of the curve to the y-axis = 0 (Kumar et al. 1999). In this study, the bandgap energy of g-C_3N_4/TiO_2 nanocomposite was found to be 2.83 eV (Fig. 6a). Due to the combination of g-C_3N_4 and TiO_2, the g-C_3N_4/TiO_2 own a smaller bandgap than pure TiO_2, making this nanocomposite photocatalyst active under visible light. It is well known that pure TiO_2 is not active under visible light due to their large bandgap energy (3.2 eV), as studied by many researchers (Zangeneh et al. 2015; Colmenares et al. 2016).

The repeatability test of TiO_2/g-C_3N_4 nanocomposite for MB degradation was carried out for five cycles and the result obtained is shown in Fig. 6b. First three cycles show nearly consistent degradation rate of MB with more than 95% indicating that the TiO_2/g-C_3N_4 nanocomposite have a good cycling stability within three cycles. However, a loss of about 10% and 15% was observed in the fourth and fifth cycles, respectively (Fig. 6b). The possible reasons might be due to the mass loss of catalyzing species after application in several cycles during washing and separation for recycling of the photocatalyst (Faisal et al. 2021).

To study the role of •OH and •O_2 towards the photocatalytic degradation of MB dye, the scavengers were added into the reaction system of the g-C_3N_4/TiO_2 nanocomposite photocatalyst. As shown in Fig. 7a, the MB photodegradation was decreased to 55.50% and 43.20% after 2 h

Table 2 Photodegradation of MB under visible-light irradiation using synthesized g-C_3N_4/TiO_2 nanocomposite and other photocatalysts

Photocatalyst	MB photodegradation	References
g-C_3N_4/TiO_2	100% after 120 min	This study
CdSe-graphene/SiO_2	100% after 180 min	Nguyen et al. (2018)
CdSe/NS graphene/Fe_3O_4	63.18% after 120 min	Khataee et al. (2019)
RGO/CdS	96.0% after 250 min	Gawande and Thakare (2013)
Fe/CdSe	79% after 150 min	Sridevi et al. (2019)
Fe/TiO_2/MWCNT	55.45% after 240 min	Hossain et al. (2018)

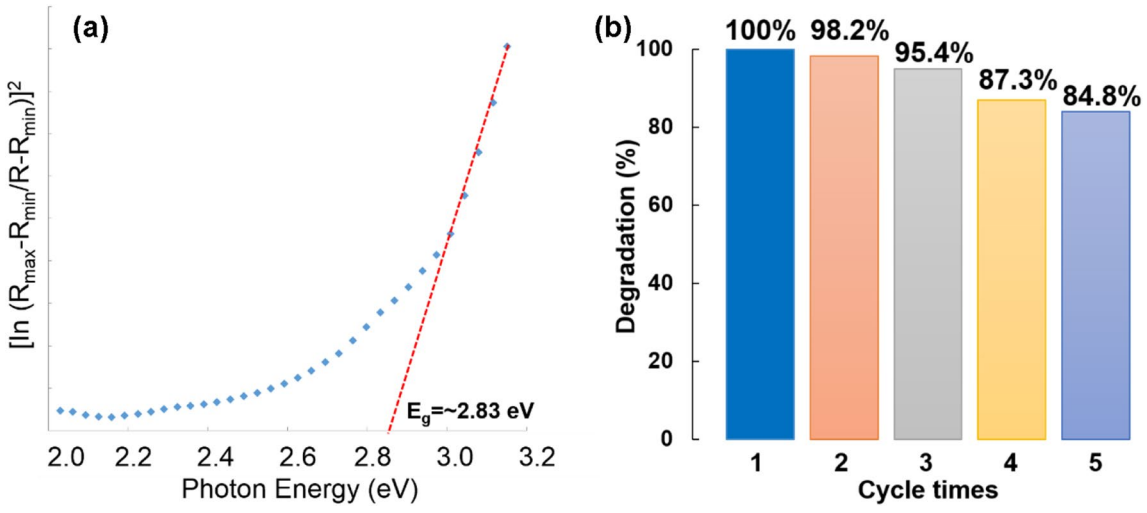

Fig. 6 **a** Energy bandgap of g-C_3N_4/TiO_2 and **b** repeatability test of g-C_3N_4/TiO_2 nanocomposite photocatalyst for MO degradation under visible-light irradiation

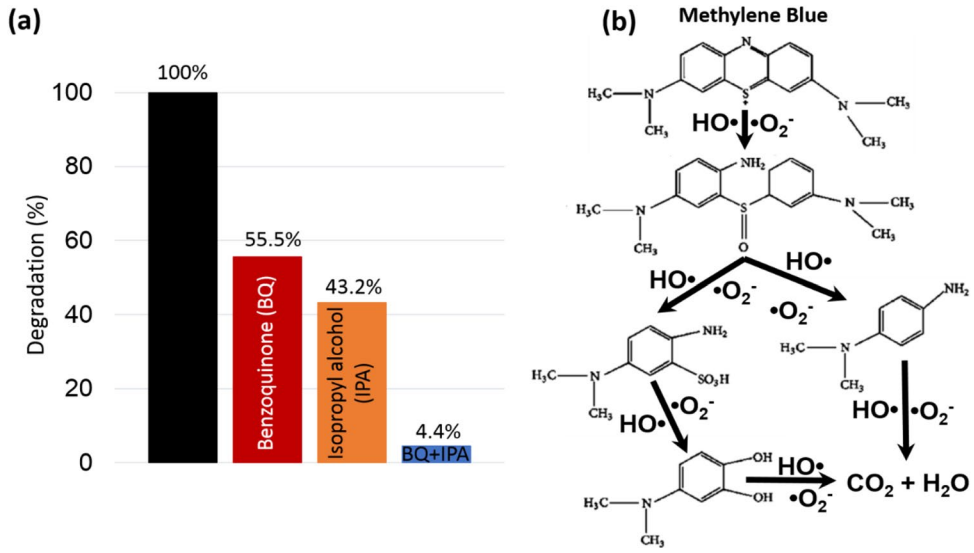

Fig. 7 **a** Degradation rate without and with scavenger, **b** mechanism of MB by •OH and $•O_2$ using g-C_3N_4/TiO_2 nanocomposite photocatalyst

irradiation with the presence of benzoquinone (BQ) and isopropyl alcohol (IPA) scavengers, respectively. This is because BQ acts as trapper of $·O_2$, while IPA inhibits the formation of •OH in the reaction system, thus reduces the presence of ROS, and consequently, the photodegradation rate. This findings suggesting that both reactive oxygen species of ·OH and $•O_2$ play a significant role in the photodegradation of MB dye. Moreover, with the presence of both scavengers BQ and IPA in the reaction system, lesser photodegradation was obtained (4.40%). The mechanism of MB degradation by ·OH and $·O_2$ using g-C_3N_4/TiO_2 nanocomposite photocatalyst is shown in Fig. 7b.

Conclusion

2D/0D heterostructure g-C_3N_4/TiO_2 nanocomposite was successfully synthesized using hydrothermal method. FTIR analysis shows the presence of functional group of g-C_3N_4 and TiO2. The XRD pattern confirmed further the existence of both materials in synthesized nanocomposite. Layered-like structure (2D) of g-C_3N_4 and agglomerated TiO_2 particles (0D) were shown by SEM micrographs. This unique properties contributes to the large surface area and pore volume of g-C_3N_4/TiO_2 nanocomposite which is important for generation of more •OH and $•O_2$. These radical plays an important role in degradation of MB as 100% degradation was obtained using g-C_3N_4/TiO_2 nanocomposite after 2-h reaction.

Acknowledgements The authors are grateful to Universiti Malaysia Terengganu (UMT) for facilities and Malaysia Ministry of Higher Education for the financial support vote (FRGS/1/2019/STG07/UMT/02/2).

Declarations

Conflict of interest This study was funded by Malaysia Ministry of Higher Education vote (FRGS/1/2019/STG07/UMT/02/2) and all the authors have no conflicts of interest to declare.

References

Abdelraheem WH, Patil MK, Nadagouda MN, Dionysiou D (2019) Hydrothermal synthesis of photoactive nitrogen-and boron-codoped TiO_2 nanoparticles for the treatment of bisphenol a in wastewater: synthesis, photocatalytic activity, degradation byproducts and reaction pathways. Appl Catal B 241:598–611. https://doi.org/10.1016/j.apcatb.2018.09.039

Ahmed MA, Abou-Gamra ZM, Salem AM (2017) Photocatalytic degradation of methylene blue dye over novel spherical mesoporous Cr_2O_3/TiO_2 nanoparticles prepared by sol-gel using octadecylamine template. J Environ Chem Eng 5:4251–4261. https://doi.org/10.1016/j.jece.2017.08.014

Antunes A, Popelka A, Aljarod O, Hassan MK, Luyt AS (2020) Effects of Rutile–TiO_2 nanoparticles on accelerated weathering degradation of poly (lactic acid). Polymers 12:1096. https://doi.org/10.3390/polym12051096

Chegeni M, Mousavi Z, Soleymani M, Dehdashtian S (2020) Removal of aspirin from aqueous solutions using graphitic carbon nitride nanosheet: theoretical and experimental studies. Diamond Relat Mater 101:107621. https://doi.org/10.1016/j.diamond.2019.107621

Chen Y, Liu X, Hou L, Guo X, Fu R, Sun J (2020) Construction of covalent bonding oxygen-doped carbon nitride/graphitic carbon nitride Z-scheme heterojunction for enhanced visible-light-driven H_2 evolution. Chem Eng J 383:123132. https://doi.org/10.1016/j.cej.2019.123132

Colmenares JC, Ouyang W, Ojeda M, Kuna E, Chernyayeva O, Lisovytskiy D, De S, Luque R, Balu AM (2016) Mild ultrasound-assisted synthesis of TiO_2 supported on magnetic nanocomposites for selective photo-oxidation of benzyl alcohol. Appl Catal B 183:107–112. https://doi.org/10.1016/j.apcatb.2015.10.034

Dong F, Wang ZY, Sun YJ, Ho WK, Zhang HD (2013) Engineering the nanoarchitecture and texture of polymeric carbon nitride semiconductor for enhanced visible light photocatalytic activity. J Colloid Interf Sci 401:70–79. https://doi.org/10.1016/j.jcis.2013.03.034

Dong G, Zhang Y, Pan Q, Qiu J (2014) A fantastic graphitic carbon nitride (g-C_3N_4) material: electronic structure, photocatalytic and photoelectronic properties. J Photochem Photobiol C 20:33–50. https://doi.org/10.1016/j.jphotochemrev.2014.04.002

Faisal M, Alsaiari M, Rashed MA, Harraz FA (2021) Biomass-derived active Carbon@ ZnO/SnO_2 novel visible-light photocatalyst for rapid degradation of linezolid antibiotic and imidacloprid insecticide. J Taiwan Inst Chem Eng 120:313–324. https://doi.org/10.1016/j.jtice.2021.03.015

Fang Y, Huang W, Yang S, Zhou X, Ge C, Gao Q, Zhang FY, S, (2020) Facile synthesis of anatase/rutile TiO_2/g-C_3N_4 multi-heterostructure for efficient photocatalytic overall water splitting. Int J Hydrog Energy 45:17378–17387. https://doi.org/10.1016/j.ijhydene.2020.04.214

Gahlot S, Dappozze F, Mishra S, Guillard C (2021) High surface area g-C_3N_4 and g-C_3N_4-TiO_2 photocatalytic activity under UV and visible light: Impact of individual component. J Environ Chem Eng 9:105587. https://doi.org/10.1016/j.jece.2021.105587

Gawande S, Thakare SR (2013) One-pot sonochemical synthesis of cds-reduced graphene oxide composite and its application for photocatalytic degradation of methylene blue. Indian J Chem 52:614–618

Goutam SP, Saxena G, Singh V, Yadav AK, Bharagava RN, Thapa KB (2018) Green synthesis of TiO_2 nanoparticles using leaf extract of *Jatropha curcas* L. for photocatalytic degradation of tannery wastewater. Chem Eng J 336:386–396. https://doi.org/10.1016/j.cej.2017.12.029

Hao M, Li Y, Gao L, Ji C, Qu R, Yang Z, Sun C, Zhang Y (2020) In-situ hard template synthesis of mesoporous carbon/graphite carbon nitride (C/CN-Tx) composites with high photocatalytic activities under visible light irridation. Solid State Sci 109:106428. https://doi.org/10.1016/j.solidstatesciences.2020.106428

Hong Y, Wang L, Liu E, Chen J, Wang Z, Zhang S, Lin X, Duan X, Shi J (2020) A curly architectured graphitic carbon nitride (g-C_3N_4) towards efficient visible-light photocatalytic H2 evolution. Inorg Chem Front 7:347–355. https://doi.org/10.1039/C9QI01128E

Hossain MA, Elias M, Sarker DR, Diba ZR, Mithun JM, Azad MAK, Siddiquey IA, Rahman MM, Uddin J, Uddin MN (2018) Synthesis of Fe-or Ag-doped TiO_2–MWCNT nanocomposite thin films and their visible-light-induced catalysis of dye degradation and antibacterial activity. Res Chem Intermed 44:2667–2683. https://doi.org/10.1007/s11164-018-3253-z

Kang S, Huang W, Zhang L, He M, Xu S, Sun D, Jiang X (2018) Moderate bacterial etching allows scalable and clean delamination of g-C_3N_4 with enriched unpaired electrons for highly improved photocatalytic water disinfection. ACS Appl Mater Interfaces 10:13796–13804. https://doi.org/10.1021/acsami.8b00007

Khataee A, Sajjadi S, Hasanzadeh A, Joo SW (2019) Synthesis of magnetically reusable Fe_3O_4 nanospheres-N, S co-doped graphene quantum dots enclosed CdSe its application as a photocatalyst. J Ind Eng Chem 75:230–237. https://doi.org/10.1016/j.jiec.2019.01.048

Kumar V, Sharma SK, Sharma TP, Singh V (1999) Band gap determination in thick films from reflectance measurements. Opt Mater 12:115–119. https://doi.org/10.1016/S0925-3467(98)00052-4

Li Q, Zhao T, Li M, Li W, Yang B, Qin D, Lv K, Wang X, Wu L, Wu X, Sun J (2019a) One-step construction of Pickering emulsion via commercial TiO_2 nanoparticles for photocatalytic dye degradation. Appl Catal B 249:1–8. https://doi.org/10.1016/j.apcatb.2019.02.057

Li F, Dong Y, Dai Q, Nguyen TT, Guo M (2019b) Novel freestanding core-shell nanofibrillated cellulose/polypyrrole/tubular graphitic carbon nitride composite film for supercapacitors electrodes. Vacuum 161:283–290. https://doi.org/10.1016/j.vacuum.2018.12.046

Li G, Liang H, Xu G, Li C, Bai J (2020) Controllable synthesized heterojunction hollow nanotube of g-C3N4/CdS: enhance visible light catalytic performance for hydrogen production. J Phys Chem Solids 145:109549. https://doi.org/10.1016/j.jpcs.2020.109549

Muhmood T, Uddin A (2020) Fabrication of spherical-graphitic carbon nitride via hydrothermal method for enhanced photo-degradation ability towards antibiotic. Chem Phys Lett. https://doi.org/10.1016/j.cplett.2020.137604

Nguyen DCT, Zhu L, Zhang Q, Cho KY, Oh WC (2018) A new synergetic mesoporous silica combined to CdSe-graphene nanocomposite for dye degradation and hydrogen evolution in visible light. Mater Res Bull 107:14–27. https://doi.org/10.1016/j.materresbull.2018.07.006

Razali MH, Yusof M (2018) Highly efficient CuO loaded TiO_2 nanotube photocatalyst for CO_2 photoconversion. Mater Lett 221:168–171. https://doi.org/10.1016/j.matlet.2018.03.100

Razali M, Ismail NA, Zulkafli MFAM, Mat Amin KA (2018) 3D Nanostructured materials: TiO_2 nanoparticles incorporated gellan gum scaffold for photocatalyst and biomedical applications. Mater Res Express 5:035039

Razali MH, Mohd Noor AF, Yusoff M (2020a) Physicochemical properties of a highly efficient Cu-ion-doped TiO_2 nanotube photocatalyst for the degradation of methyl orange under sunlight. J Nanosci Nanotechnol 20:965–972. https://doi.org/10.1166/jnn.2020.16944

Razali MH, Ismail NA, Amin KAM (2020b) Titanium dioxide nanotubes incorporated gellan gum bio-nanocomposite film for wound healing: effect of TiO_2 nanotubes concentration. Int J Biol Macromol 153:1117–1135. https://doi.org/10.1016/j.ijbiomac.2019.10.242

Sathiyan K, Bar-Ziv R, Mendelson O, Zidki T (2020) Controllable synthesis of TiO_2 nanoparticles and their photocatalytic activity in dye degradation. Mater Res Bull. https://doi.org/10.1016/j.materresbull.2020.110842

Sridevi DV, Sundaravadivel E, Kanagaraj P (2019) Influence of Fe doping on structural, physicochemical and biological properties of CdSe nanoparticles. Mater Sci Semicond Process 101:67–75. https://doi.org/10.1016/j.mssp.2019.05.031

Sun Y, Gao Y, Zeng J, Guo J, Wang H (2020) Enhancing visible-light photocatalytic activity of Ag-TiO_2 nanowire composites by one-step hydrothermal process. Mater Lett. https://doi.org/10.1016/j.matlet.2020.128506

Tan X, Wang X, Hang H, Zhang D, Zhang N, Xiao Z, Tao H (2019) Self-assembly method assisted synthesis of g-C_3N_4/ZnO heterostructure nanocomposites with enhanced photocatalytic performance. Opt Mater 96:109266. https://doi.org/10.1016/j.optmat.2019.109266

Tian Y, Chang B, Lu J, Fu J, Xi F, Dong X (2013) Hydrothermal synthesis of graphitic carbon nitride–Bi_2WO_6 heterojunctions with enhanced visible light photocatalytic activities. ACS Appl Mater Interfaces 5:7079–7085. https://doi.org/10.1021/am4013819

Wang K, Fu J, Zheng Y (2019) Insights into photocatalytic CO_2 reduction on C_3N_4: Strategy of simultaneous B, K co-doping and enhancement by N vacancies. Appl Catal B Environ 254(2019):270–282

Warkhade SK, Zodape SP, Pratap UR, Wankhade AV (2019) Rutile TiO_2/CoSe nanocomposite: an efficient photocatalyst for photodegradation of model organic dyes under visible light irradiation. J Mol Liq 279:434–443. https://doi.org/10.1016/j.molliq.2018.12.119

Zangeneh H, Zinatizadeh AAL, Habibi M, Akia M, Hasnain Isa M (2015) Photocatalytic oxidation of organic dyes and pollutants in wastewater using different modified titanium dioxides: a comparative review. J Ind Eng Chem 26:1–36. https://doi.org/10.1016/j.jiec.2014.10.043

Zhang M, Duan Y, Jia H, Wang F, Wang L, Su Z, Wang C (2017) Defective graphitic carbon nitride synthesized by controllable co-polymerization with enhanced visible light photocatalytic hydrogen evolution. Catal Sci Technol 7:452–458. https://doi.org/10.1039/C6CY02318E

Zheng R, Li C, Zhang C, Wang W, Wang L, Feng L, Bian J (2020) Photo-reduction of NO by g-C_3N_4@ foamed ceramic. Chin J Chem Eng 28:1840–1846. https://doi.org/10.1016/j.cjche.2020.02.02